

# Altered Brain Endothelial Cell Phenotype from a Familial Alzheimer Mutation and Its Potential Implications for Amyloid Clearance and Drug Delivery

Lotta E. Oikari,<sup>1,8</sup> Rucha Pandit,<sup>2,8</sup> Romal Stewart,<sup>1</sup> Carla Cuni-López,<sup>1</sup> Hazel Quek,<sup>1</sup> Ratneswary Sutharsan,<sup>1,2</sup> Laura M. Rantanen,<sup>1</sup> Minna Oksanen,<sup>4</sup> Sarka Lehtonen,<sup>3,4</sup> Carmela Maria de Boer,<sup>5,6</sup> Jose M. Polo,<sup>5,6,7</sup> Jürgen Götz,<sup>2</sup> Jari Koistinaho,<sup>3,4,9</sup> and Anthony R. White<sup>1,9,\*</sup>

<sup>1</sup>Mental Health Program, QIMR Berghofer Medical Research Institute, Brisbane, QLD, Australia

<sup>2</sup>Clem Jones Centre for Ageing Dementia Research, Queensland Brain Institute, The University of Queensland, Brisbane, QLD, Australia

<sup>3</sup>Neuroscience Center, Helsinki Institute of Life Science, University of Helsinki, Helsinki, Finland

<sup>4</sup>A.I. Virtanen Institute for Molecular Sciences, University of Eastern Finland, Kuopio, Finland

<sup>5</sup>Department of Anatomy and Developmental Biology, Monash University, Melbourne, VIC, Australia

<sup>6</sup>Development and Stem Cells Program, Monash Biomedicine Discovery Institute, Clayton, VIC, Australia

<sup>7</sup>Australian Regenerative Medicine Institute, Monash University, Melbourne, VIC, Australia

<sup>8</sup>Co-first author

<sup>9</sup>Co-senior author

\*Correspondence: [tony.white@qimrberghofer.edu.au](mailto:tony.white@qimrberghofer.edu.au)

<https://doi.org/10.1016/j.stemcr.2020.03.011>

## SUMMARY

The blood-brain barrier (BBB) presents a barrier for circulating factors, but simultaneously challenges drug delivery. How the BBB is altered in Alzheimer disease (AD) is not fully understood. To facilitate this analysis, we derived brain endothelial cells (iBECs) from human induced pluripotent stem cells (hiPSCs) of several patients carrying the familial AD *PSEN1* mutation. We demonstrate that, compared with isogenic *PSEN1* corrected and control iBECs, AD-iBECs exhibit altered tight and adherens junction protein expression as well as efflux properties. Furthermore, by applying focused ultrasound (FUS) that transiently opens the BBB and achieves multiple therapeutic effects in AD mouse models, we found an altered permeability to 3–5 kDa dextran as a model cargo and the amyloid- $\beta$  (A $\beta$ ) peptide in AD-iBECs compared with control iBECs. This presents human-derived *in vitro* models of the BBB as a valuable tool to understand its role and properties in a disease context, with possible implications for drug delivery.

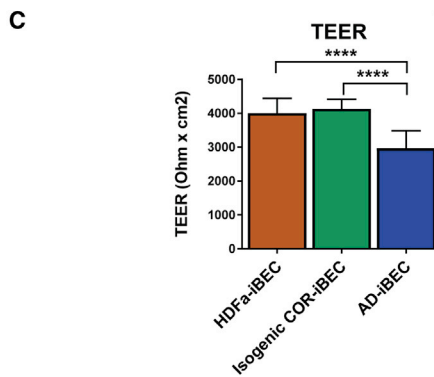
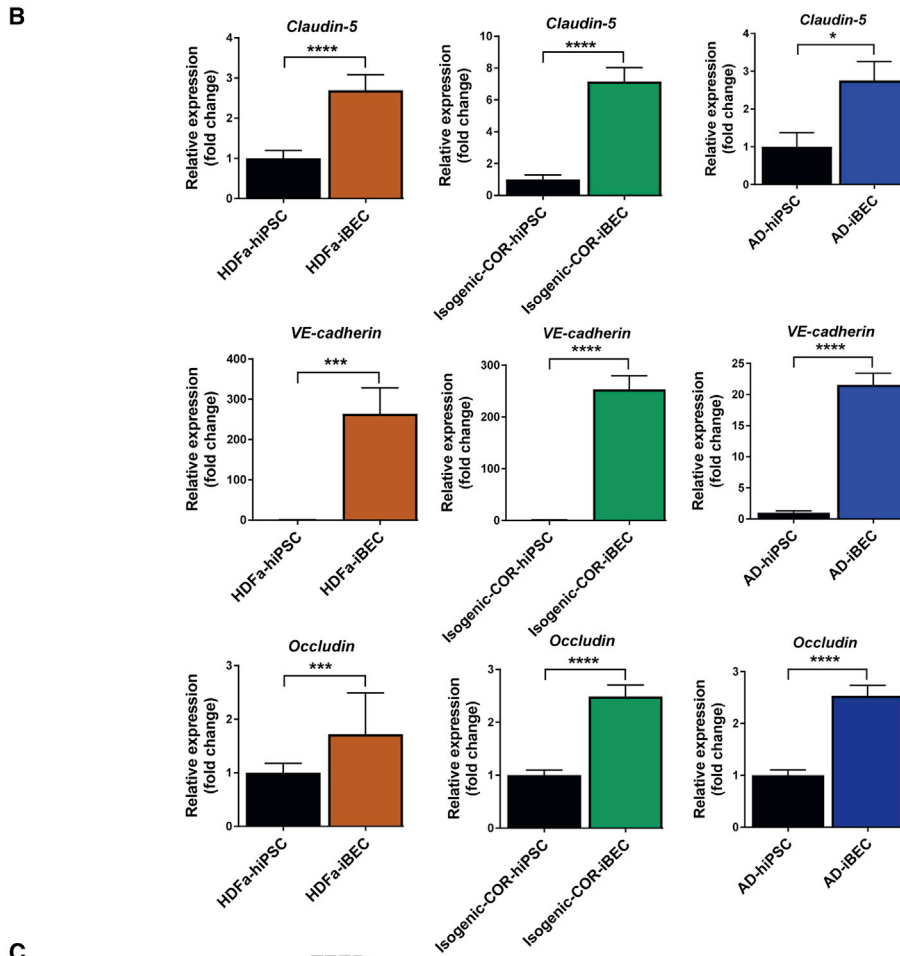
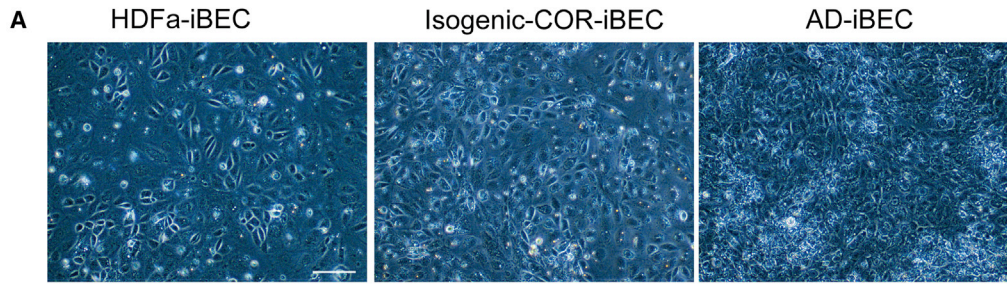
## INTRODUCTION

Treatment of neurodegenerative diseases is challenged by limited passage of therapeutic drugs across the blood-brain barrier (BBB) to the brain (Pandit et al., 2019a; Sweeney et al., 2018). The BBB lines the walls of brain microvessels and is critical to prevent entry of toxic molecules and facilitate uptake of nutrients (Zenaro et al., 2017). The functional BBB or neurovascular unit is formed by brain endothelial cells (BECs), pericytes, astrocytes, and neurons, with BEC-expressed tight junctions inhibiting the entry of unwanted molecules into the central nervous system (CNS) (Zenaro et al., 2017). BBB-specific tight junction proteins (TJPs) and adherens junction proteins include occludin, claudins (claudin-3 and claudin-5), ZO-1, and VE-cadherin (Li et al., 2018; Sweeney et al., 2018). BEC-expressed efflux transporters, such as P-glycoprotein (P-gp), multidrug resistance proteins (MRPs), and breast cancer resistance protein (BCRP) actively pump molecules back into the blood (Qosa et al., 2015). Uptake transporters, such as glucose transporter 1 (GLUT-1), ensure the uptake of vital nutrients into the CNS (Devraj et al., 2011).

Several neurodegenerative diseases, including Alzheimer disease (AD), have been claimed to be associated with an abnormal BBB (reviewed in Sweeney et al., 2018). AD is a complex disorder characterized by amyloid- $\beta$  (A $\beta$ ) plaques

and tau-containing neurofibrillary tangles, leading to a gradual decline of cognition (Polanco et al., 2018). The majority of AD cases are sporadic (late onset) of unknown etiology, with less than 1% of familial AD (FAD) cases of known genetic cause and early onset (Ryan et al., 2016). Multiple FAD mutations occur in genes encoding the amyloid precursor protein (*APP*), presenilin-1 (*PSEN1*), and presenilin-2 (*PSEN2*) (Ryan et al., 2016). Currently, there is no cure for AD and therapeutic development is slowed by poor delivery of compounds across the BBB (Frozza et al., 2018; Pandit et al., 2019a; Sweeney et al., 2018).

There are multiple changes to the BBB in AD, indicated by the presence of blood-borne substances and circulating leukocytes in the CNS (Hultman et al., 2013; Nelson et al., 2016; Zenaro et al., 2015). BEC and pericyte degeneration, and cerebrovascular pathology have also been described in AD patients and mouse models (reviewed in Gama Sosa et al., 2010; Montagne et al., 2017; Sweeney et al., 2018). Reduced BBB integrity is associated with neuroinflammation, neuronal injury, oxidative stress, and faulty clearance of A $\beta$ , as well as altering uptake of therapeutics (reviewed in Sweeney et al., 2018). However, there is also a recent study claiming no differences in BBB permeability in human AD and in AD mouse models (Bien-Ly et al., 2015), highlighting the lack of understanding of BBB-specific changes in AD and what their impact is on drug delivery.



(legend on next page)



Although a disrupted BBB is considered an opportunity to more easily deliver drugs into the brain, the altered physiological conditions in the AD-BBB can hinder drug delivery by diffusion (Sweeney et al., 2018). This reinforces the importance of establishing AD-specific models of the human BBB to understand its contribution to AD pathogenesis and drug delivery. As a promising approach, BECs (iBECs) have been generated from human induced pluripotent stem cells (hiPSCs) (Lippmann et al., 2014). hiPSC-derived iBECs express key proteins of BECs, demonstrate high barrier integrity and exhibit efflux transporter activity characteristic of the BBB *in vivo* (Lippmann et al., 2014).

Focused ultrasound (FUS) is a technique that uses acoustic energy, together with gas-filled microbubbles (MBs), traditionally used as ultrasound contrast agents, to transiently open the BBB, potentially allowing for enhanced drug delivery (Leinenga et al., 2016). Opening of the BBB is achieved in part through an interaction between MBs and sound waves leading to loosening of tight junctions between BECs (Sheikov et al., 2004). Ultrasound has been used to facilitate delivery of an anti-A $\beta$  antibody to reduce plaque burden (Jordao et al., 2010) and a tau-specific antibody fragment to reduce pathological tau and improve associated behaviors (Nisbet et al., 2017). Ultrasound alone has been shown to open the BBB in mice with A $\beta$  pathology, resulting in reduction of plaque burden and restoration of memory functions, without the need for additional therapeutic agents (Leinenga and Götz, 2015). Similarly, ultrasound alone can reduce tau pathology and associated motor impairments (Pandit et al., 2019b). These results strongly support the use of low-intensity FUS as a potential therapeutic modality for AD; however, the effects of FUS in a human BBB disease model remain unexplored.

Here, we used hiPSCs derived from FAD patients with a *PSEN1* exon 9 deletion (Oksanen et al., 2017) along with isogenic *PSEN1*-corrected as well as healthy controls to study AD-specific differences in human BECs, previously not described in the literature. We also investigated the potential of human iBECs to model the effects of FUS on BBB opening. Our results identify key phenotypical differences between AD- and control (ctrl)-iBECs and demonstrate the differential effects of FUS on BBB opening in AD- and ctrl-iBECs.

## RESULTS

### Ctrl- and AD-iPSCs Readily Differentiate into iBECs

iBECs were differentiated from three FAD iPSC lines carrying the *PSEN1*  $\Delta E9$  mutation (AD-iBECs), two isogenic control iPSC lines where the *PSEN1* mutation had been corrected (isogenic COR-iBEC) (Oksanen et al., 2017), and one unrelated control iPSC line generated from human dermal fibroblasts (HDFa-iBEC). iBEC differentiation was achieved using previously established protocols with some modifications (Lippmann et al., 2014; Stebbins et al., 2016; Qian et al., 2017). Following purification on plates coated with collagen IV and fibronectin, all lines displayed endothelial cell morphology, indicated by a cobblestone-like appearance (Figures 1A and 2A). Compared with undifferentiated hiPSCs, iBECs generated from all lines expressed higher levels of endothelial cell and BBB TJP marker genes for occludin, VE-cadherin, and claudin-5 (Figure 1B). To confirm the integrity of the iBEC monolayer, the cells were cultured on Transwell inserts and the trans-endothelial electrical resistance (TEER) was measured. The mean TEER across the iBEC lines reflected levels previously published for iBECs (Lippmann et al., 2014): HDFa-iBEC 4,000  $\Omega/\text{cm}^2$ ; AD-iBEC 2,900  $\Omega/\text{cm}^2$ ; and isogenic COR-iBEC 4,100  $\Omega/\text{cm}^2$ . AD-iBECs exhibited a lower TEER compared with HDFa- and isogenic COR-iBECs (Figures 1C, and S2C). The HDFa- and the two isogenic COR-iBECs showed similar properties. To streamline the subsequent analyses of phenotypical differences, we combined and averaged the data from these three control cell lines and termed them “combined iBEC” (meaning combined control iBECs).

### AD-iBECs Express Altered mRNA Levels of TJPs Compared with Combined Ctrl-iBECs

With both tight and adherens junctions playing a central role in BBB integrity, we examined and compared their expression between the two experimental groups. Immunofluorescence for occludin and claudin-5, which were ubiquitously expressed in all iBEC lines, displayed distinct localization to cell borders, confirming iBEC specification (Figures 2A and S2). We then compared levels of mRNA encoding BBB-specific TJP and adherens junction proteins between the combined ctrl-iBECs and AD-iBECs (Figure 2B).

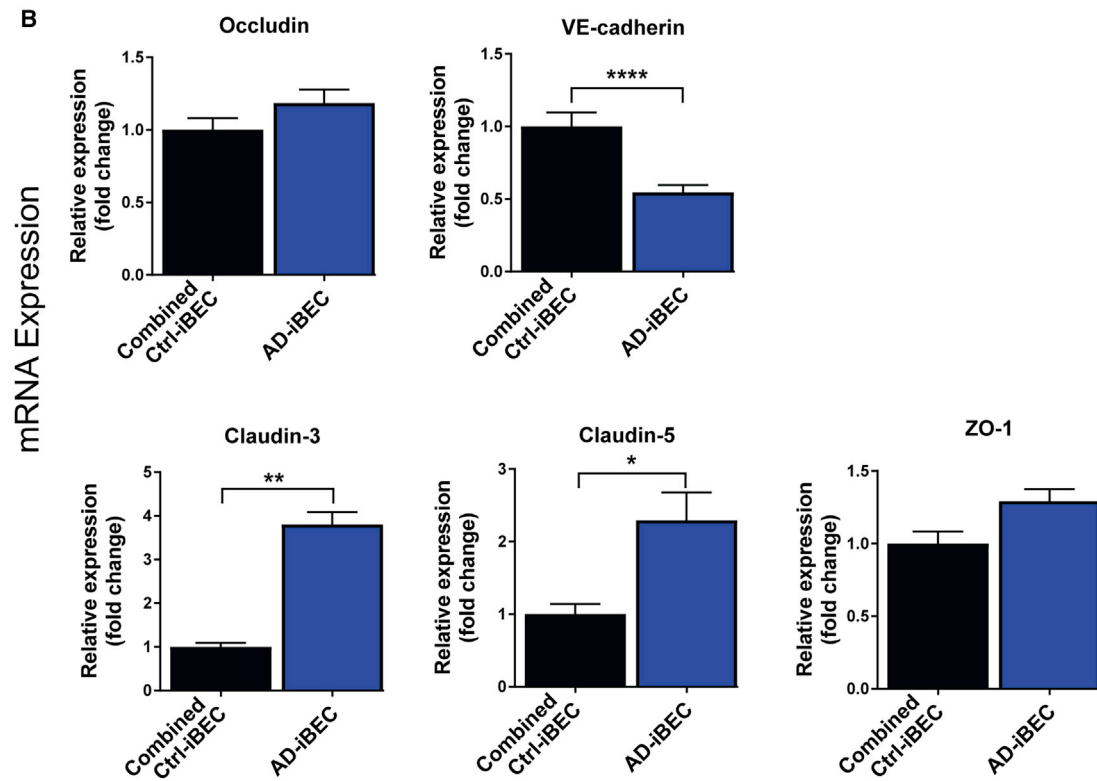
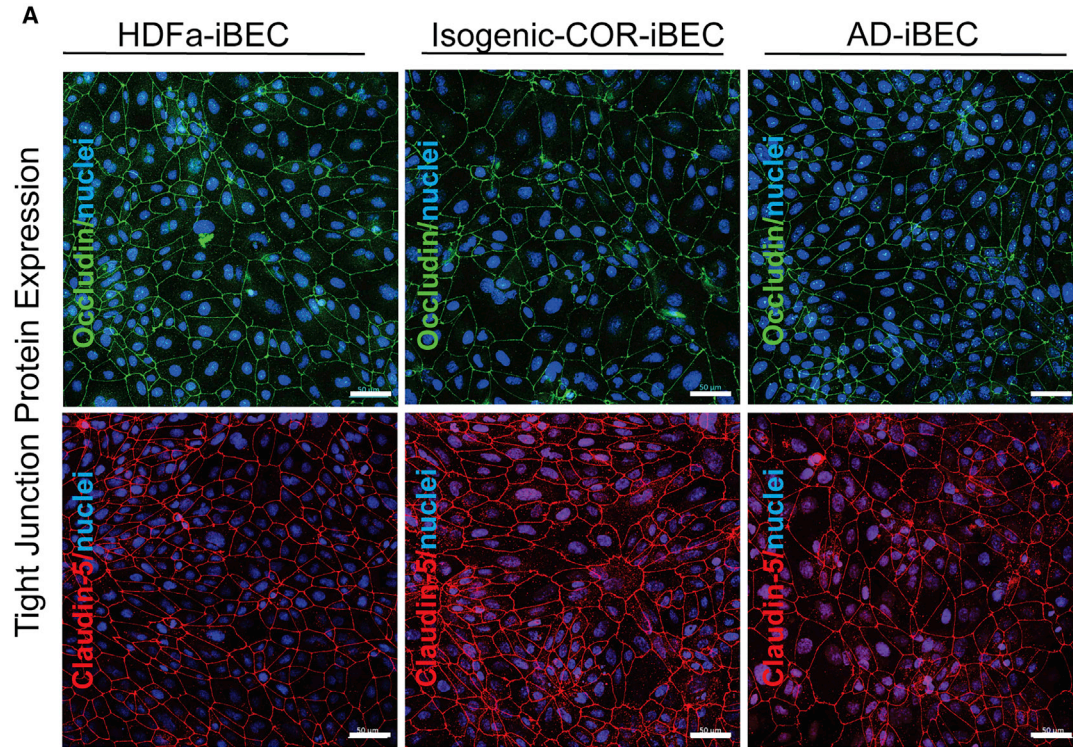
#### Figure 1. Differentiation of hiPSCs into iBECs

(A) Phase-contrast images of iBECs derived from control (HDFa), isogenic *PSEN1*-corrected control (isogenic COR), and *PSEN1* mutant AD hiPSCs (20 $\times$  magnification). Scale bar, 50  $\mu\text{m}$ .

(B) Relative expression of mRNA for occludin, VE-cadherin, and claudin-5 in HDFa-, isogenic COR-, and AD-iBECs shown as fold change to undifferentiated hiPSCs (HDFa:  $n = 1$  line, isogenic COR;  $n = 2$  lines, AD:  $n = 3$  lines, 6 independent replicates).

(C) Trans-endothelial electrical resistance (TEER) in HDFa-, isogenic COR-, and AD-iBECs shown as  $\Omega/\text{cm}^2$  (ctrl:  $n = 1$  line, isogenic COR;  $n = 2$  lines, AD:  $n = 3$  lines, 18 technical replicates from  $n = 3$  independent experiments).

Data are presented as mean  $\pm$  SEM. Statistical analysis between two groups was performed using Student's t test and between multiple groups using one-way ANOVA, \* $p < 0.05$ , \*\*\* $p < 0.001$ , \*\*\*\* $p < 0.0001$ .



(legend on next page)



mRNA levels of the occludin gene did not differ between combined ctrl- and AD-iBECs, although a slightly increased expression (fold change 1.2,  $p = 0.055$ ) was identified in AD-iBECs compared with combined ctrl-iBECs (Figure 2B). mRNA for adherens junction protein VE-cadherin was expressed at a lower level in AD-iBECs compared with combined ctrl-iBECs (Figure 2B). The opposite was seen for claudin-3 and claudin-5 mRNA, which were more highly expressed in AD-iBECs compared with combined ctrl-iBECs (Figure 2B). *ZO-1*, which acts as a TJ scaffolding protein was not differentially expressed, although it demonstrated slightly increased expression (fold change 1.3,  $p = 0.06$ ) in AD-iBECs (Figure 2B). These results demonstrate complex effects of *PSEN1* mutation on TJP mRNA expression.

### AD-iBECs Exhibit Reduced BBB Transporter Expression and Increased Activity Compared with Combined Ctrl-iBECs

Uptake and efflux transporters play a key role in nutrient uptake of the brain and in expelling unwanted molecules back to the blood, respectively (Devraj et al., 2011; Qosa et al., 2015). We therefore analyzed transporter expression and activity in ctrl- and AD-iBECs. *GLUT-1* (responsible for glucose uptake), was found to be ubiquitously expressed in the plasma membrane in HDFa-, isogenic COR-, and AD-iBECs (Figures 3A and S3) and did not demonstrate differential expression between the iBEC lines at the mRNA level (Figure 3B). Interestingly, mRNA levels of the efflux transporter *P-GP* were lower in AD-iBECs when compared with combined ctrl-iBECs (Figure 3C). However, this did not correlate with significantly altered P-gp-dependent accumulation of rhodamine 123 in AD-iBECs, although a trend toward increased accumulation was observed (Figure 3D) (see Supplemental Information for rhodamine assay). This may reflect differences between gene and protein levels. Intriguingly, mRNA levels of the efflux transporters *MRP1*, *MRP2*, and *BCRP* were all higher in AD-iBECs compared with combined ctrl-iBECs (Figure 3E). How this relates to transporter activity remains to be investigated.

### FUS Transiently Opens the iBEC Monolayer with AD-iBECs Demonstrating Differential Opening Compared with Controls

FUS is an innovative technology, and in conjunction with gas-filled MBs has the potential to transiently open the BBB

to aid drug delivery (Nisbet et al., 2017) and reduce A $\beta$  plaque load in AD models (Leinenga and Götz, 2015). We explored the possibility to model the effects of FUS on the BBB *in vitro* using AD-iBECs. In these experiments, two AD-iBEC lines and the corresponding isogenic COR-iBEC lines (corrected) were used. Conditions included untreated (UT), ultrasound only (US), MB only, and ultrasound plus MBs (US + MB). Of note, MBs alone are considered to be biologically inert, whereas US on its own is a pressure wave that can have potential bio-effects (Leinenga et al., 2016). Cells were analyzed both immediately and 24 h after ultrasound treatment of the expression of claudin-5 and occludin, changes to TEER, and permeability to fluorescently conjugated dextran and A $\beta$ .

Immediately after treatment with US at 0.3 MPa peak rarefactional pressure (120 s), the isogenic corrected (COR)- and AD-iBEC monolayer was intact in the UT only and MB conditions, with several small cell-free patches present in the iBEC monolayer after US (Figures 4A and S4A). Following US + MB treatment, a clear disruption of the iBEC monolayer was evident in both isogenic COR- and AD-iBECs, indicated by the presence of clear cell-free patches in the cellular monolayer (Figures 4A and S4A). Intriguingly, the cell-free patches within AD-iBEC cultures were more defined and covered a smaller area than in the monolayer of isogenic COR-iBECs (Figures 4A, S4A and S4B). To investigate the functional effects of ultrasound treatment on monolayer integrity, we also measured TEER after FUS treatment on iBECs cultured in Transwells (Figures 4C and S4C). These measurements confirmed that US + MB reduced barrier integrity, with both isogenic COR- and AD-iBECs demonstrating decreased TEER in the US + MB condition (isogenic COR: fold change 0.65; AD: fold change 0.68) compared with UT, with no difference observed in the reduction of TEER between the lines (Figure 4C). Although no disruption of the iBEC monolayer was evident in the MB condition, reduced TEER was also identified in this condition compared with UT in isogenic COR-iBECs; however, TEER remained lower in the US + MB condition compared with MB (Figure S4C).

To determine if changes in TEER were associated with US + MB effect on cell-cell barrier integrity or from the appearance of cell-free spaces, we repeated the treatments at a lower rarefactional pressure of 0.15 MPa (120 s). At

### Figure 2. AD-iBECs Express Altered Levels of TJP Genes Compared with Ctrl-iBECs

(A) Representative immunofluorescence images in HDFa-, isogenic COR-, and AD-iBECs of occludin (green) and claudin-5 (red) (20 $\times$  magnification, Hoechst counterstain). Scale bar, 50  $\mu$ m. (B) Relative expression of mRNA for occludin, VE-cadherin, claudin-3, claudin-5, and *ZO-1* in combined ctrl (HDFa and isogenic COR combined)- and AD-iBECs shown as fold change to combined ctrl-iBECs (ctrl:  $n = 3$  lines, AD:  $n = 3$  lines, six independent replicates). Data are presented as mean  $\pm$  SEM. Statistical analysis was performed using Student's *t* test, \* $p < 0.05$ , \*\* $p < 0.01$ , \*\*\*\* $p < 0.0001$ . See also Figure S2.

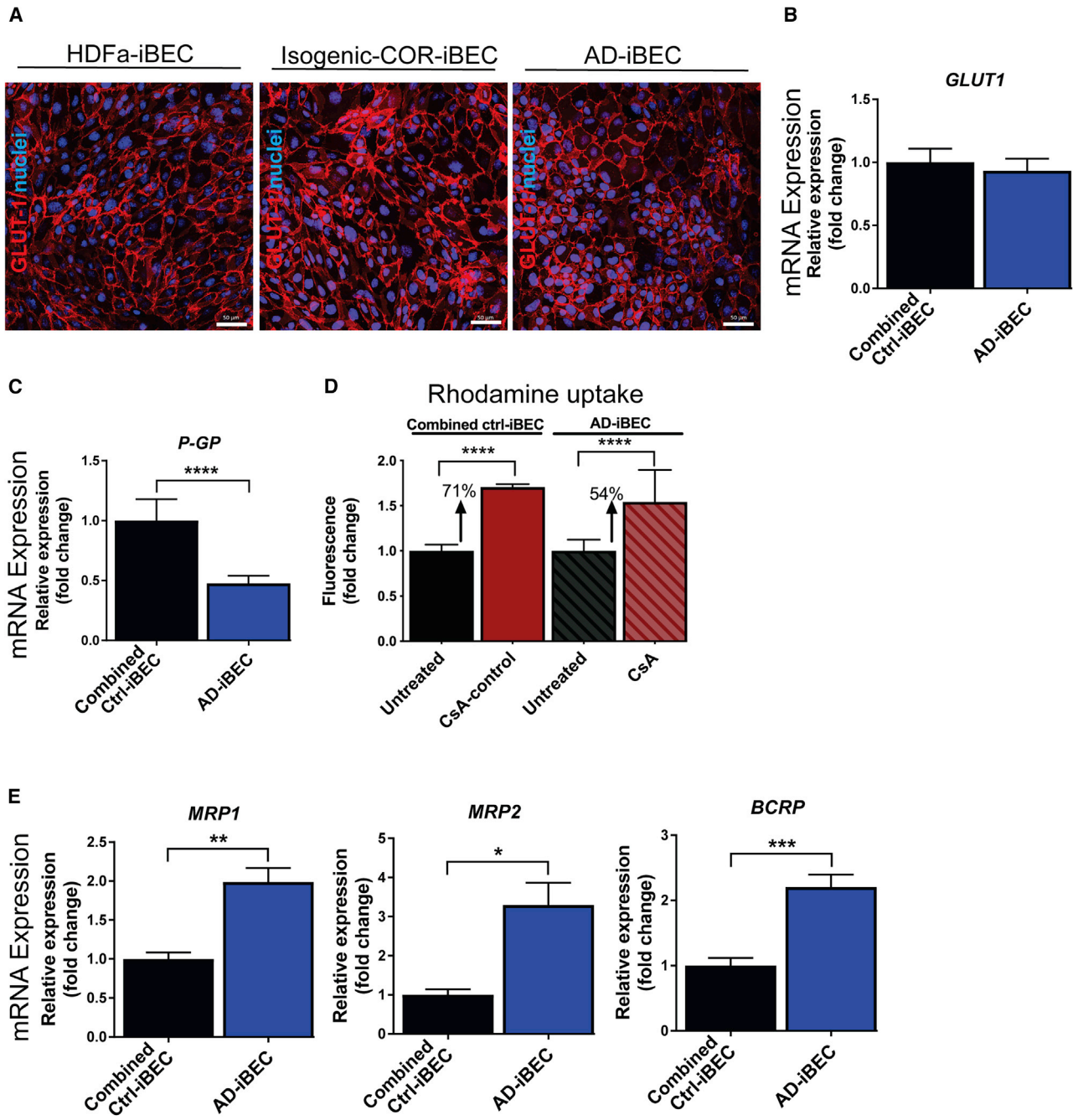


**Figure 3. AD-iBECs Exhibit Altered Expression and Function of Efflux Transporters**

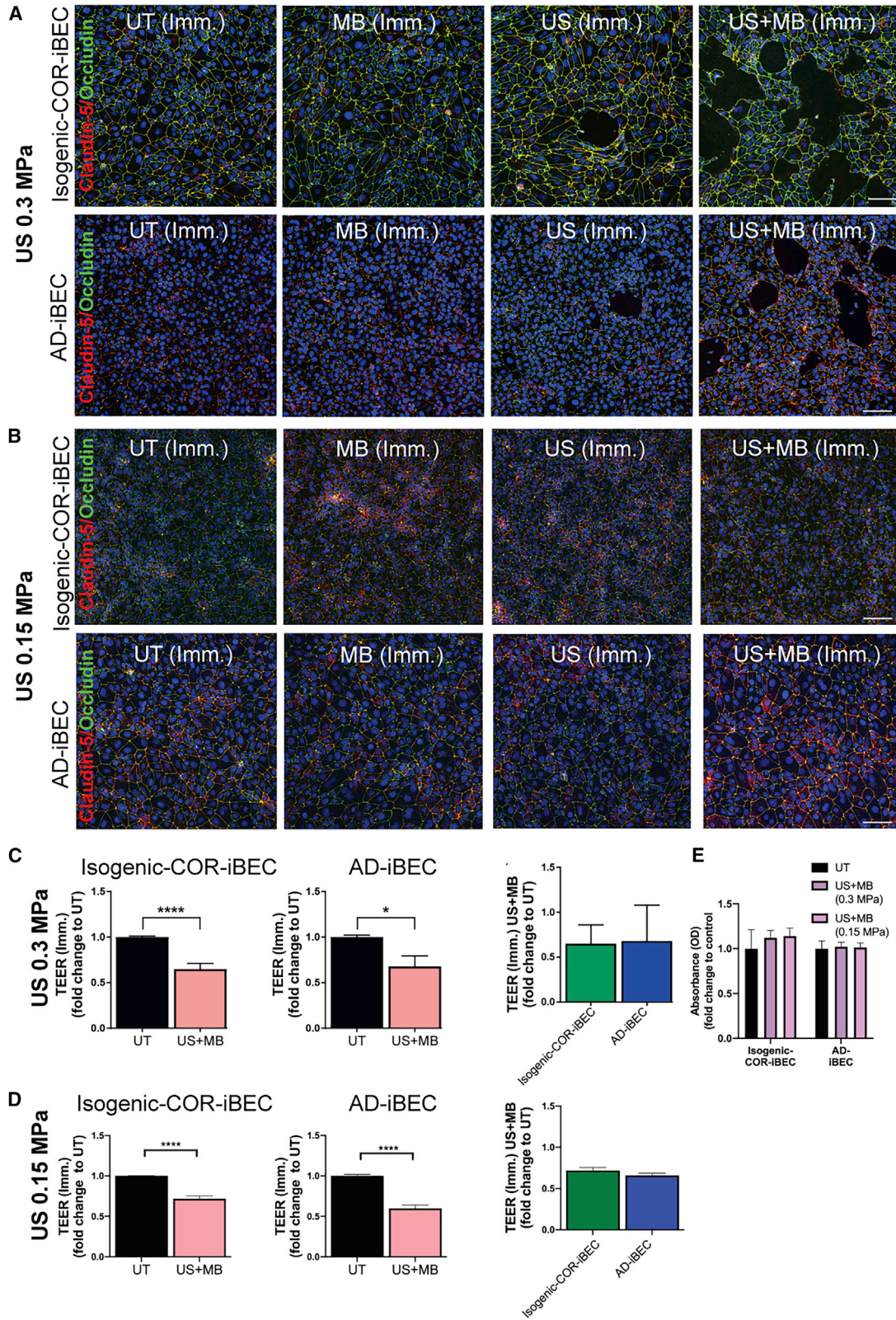
(A) Representative immunofluorescence images in control HDFa-, isogenic COR-, and AD-iBECs of GLUT-1 (red) (20× magnification, Hoechst counterstain). Scale bar, 50 μm.

(B and C) Relative gene expression of (B) *GLUT-1* and (C) *P-GP* in combined ctrl- and AD-iBECs shown as fold change to combined ctrl-iBECs (HDFa and isogenic COR combined) (ctrl: n = 3 lines, AD: n = 3 lines, 6 independent replicates).

(D) P-gp activity measured by rhodamine 123 uptake in UT- and cyclosporin A (CsA)-inhibited combined ctrl- and AD-iBECs. Graphs display fold change in fluorescence compared with untreated condition (ctrl: n = 3 lines, AD: n = 3 lines, 7 technical replicates).

(E) Relative gene expression of *MRP1*, *MRP2*, and *BCRP* in combined ctrl- and AD-iBECs shown as fold change to ctrl-iBECs (ctrl: n = 3 lines, AD: n = 3 lines, 6 independent replicates).

Data are presented as mean ± SEM. Statistical analysis was performed using Student's t test or ANOVA (D), \*p < 0.05, \*\*p < 0.01, \*\*\*p < 0.001, \*\*\*\*p < 0.0001. See also Figure S3.



(legend on next page)



this setting, no visible changes (cell-free spaces) were observed in any culture (Figure 4B). This lower US setting, however, induced the same reduction in TEER in both isogenic COR-iBECs and AD-iBECs as observed at 0.3 MPa (Figure 4D compared with Figure 4C). This was consistent with the observation that the higher setting (0.3 MPa) did not appear to adversely affect cell health. To confirm this, we performed an MTT assay for cell health, which revealed no significant change to cell viability or numbers after treatment with either 0.3 or 0.15 MPa US + MB (Figure 4E) and also found that RNA levels of AD-iBECs did not differ after UT and US + MB treatment.

Importantly, 24 h after US + MB treatment at 0.3 MPa the isogenic COR- and AD-iBEC monolayers demonstrated full recovery indicated by the absence of cell-free patches when stained for claudin-5 and occludin (Figure 5A). This was supported by TEER measurements performed 24 h after treatment, which demonstrated a slight increase in TEER in the US + MB condition compared with UT condition in both isogenic COR- and AD-iBECs and no difference in TEER between UT and other conditions (Figures 5B and S4C). Analysis of the intensity of claudin-5 and occludin staining immediately and 24 h after US + MB treatment confirmed higher claudin-5 expression in AD-iBECs compared with isogenic COR, with the AD-iBEC US + MB condition also demonstrating higher claudin-5 expression compared with the isogenic COR-iBEC US + MB condition 24 h after treatment (Figure 5C). The intensity of occludin was shown to be higher after US + MB in both iBEC lines at the immediate time point, likely indicating differential localization or clustering of this protein (Figure 5C). Higher occludin intensity was also observed in AD-iBEC US + MB condition compared with the isogenic corrected control US + MB condition 24 h after treatment (Figure 5C).

#### FUS Causes Changes in TJP mRNA Expression in AD-iBECs

We then measured the relative expression levels of the TJP genes immediately and 24 h after FUS to understand the effect of FUS on TJP expression. When analyzed immediately

(~10 s) after treatment (0.3 MPa condition), occludin, claudin-5, and *ZO-1* mRNAs were downregulated in AD-iBECs after US + MB compared with the UT condition (Figure 6A). In isogenic COR-iBECs, only *ZO-1* demonstrated decreased expression after US + MB compared with UT (Figure 6A). VE-cadherin mRNA, which was expressed at a lower level in AD-iBECs compared with isogenic COR-iBECs, demonstrated an increase in AD-iBECs after US + MB treatment compared with UT (Figure 6A).

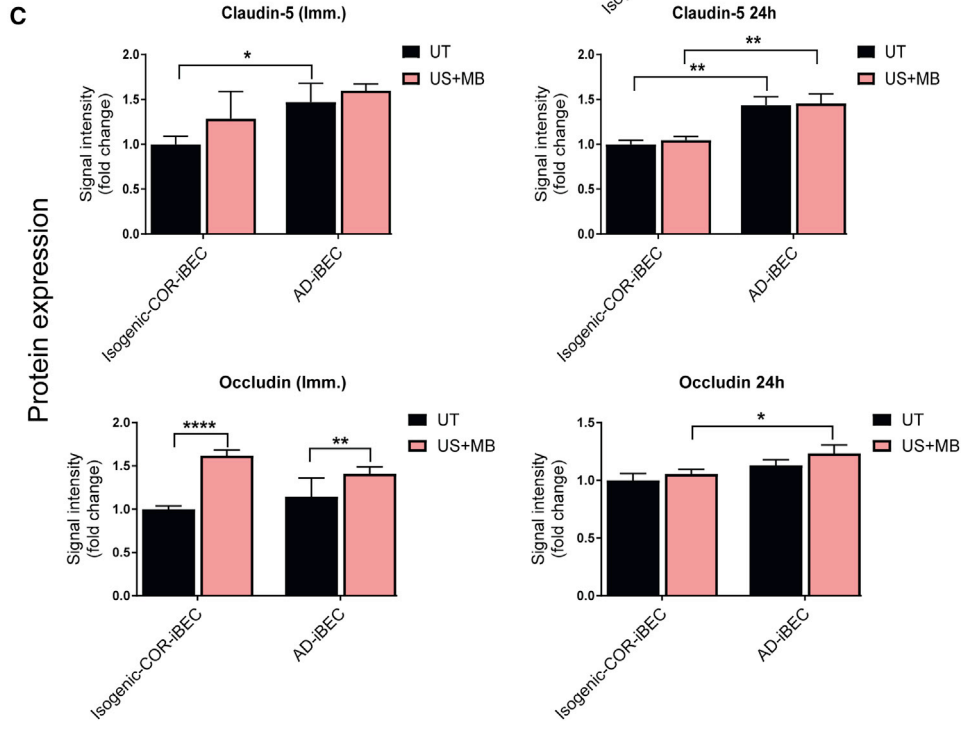
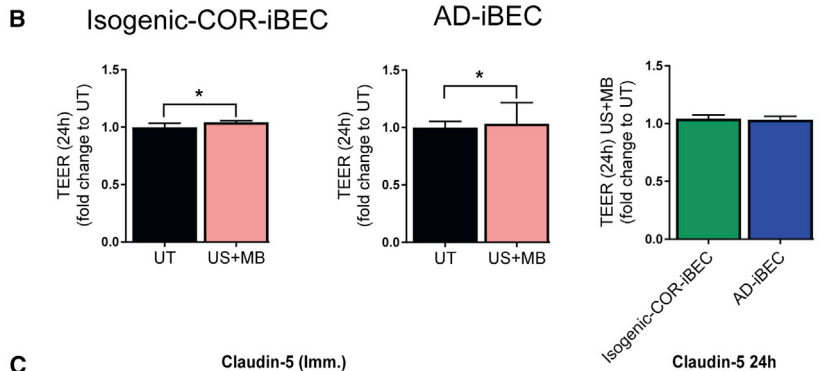
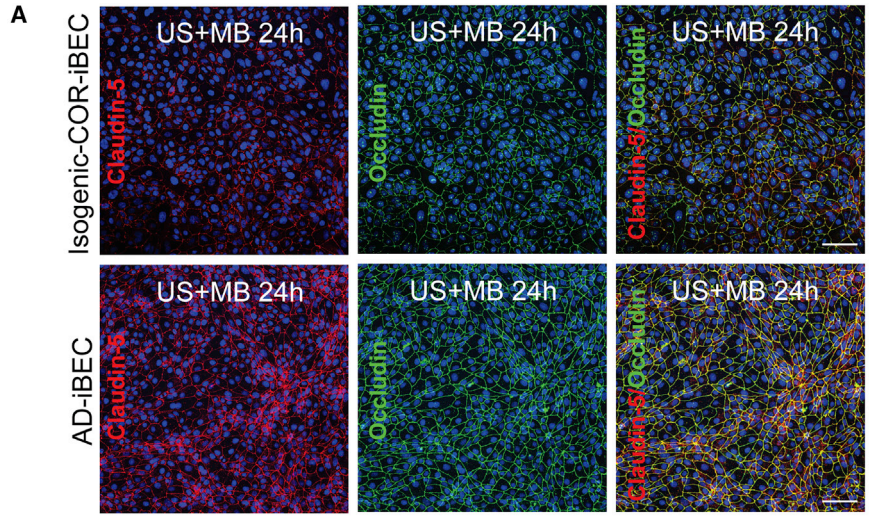
Twenty-four hours after US + MB treatment (0.3 MPa), AD-iBECs continued to demonstrate downregulated occludin, claudin-5, and *ZO-1* mRNA expression compared with UT (Figure 6B). Consistent with the immediate time point, AD-iBEC UT cells continued to express higher levels of claudin-5 and *ZO-1* mRNA and lower levels of VE-cadherin mRNA compared with isogenic COR-iBECs (Figure 6B). In isogenic COR-iBECs, mRNA for VE-cadherin was upregulated in the US + MB condition compared with UT with an elevated trend in occludin (fold change 1.1) and claudin-5 mRNA expression (fold change 1.3) (Figure 6B). These results suggest that TJP gene expression does not recover at a similar rate in AD-iBECs compared with isogenic COR-iBECs after FUS at 0.3 MPa. Given the complexity of TJP mRNA changes in response to FUS, future studies should investigate this in more detail at different pressure settings and time points post-treatment.

#### FUS Increases the Permeability of the AD-iBEC Monolayer Demonstrating Reduced Recovery in Permeability

Finally, we examined the ability of FUS to increase the permeability of the iBEC monolayer by examining the passage of the fluorescently conjugated carrier molecule dextran (sized 3–5 kDa) and A $\beta$  (1–42) (sized 4 kDa, added without pre-aggregation) through the iBEC monolayer (Figure 7A). The isogenic COR-iBEC UT condition was used as a baseline to which all the treatment conditions in both iBEC lines were compared. Immediately after treatment (0.3 MPa), consistent with the TEER measurements, the permeability to dextran was increased in the US + MB condition (fold change 2.5) in isogenic

#### Figure 4. FUS in the Presence of Microbubbles Disrupts AD-iBEC Monolayer Differently Compared with Ctrl-iBECs

(A and B) Representative immunofluorescence images of claudin-5 (red) and occludin (green) co-stained in isogenic COR- and AD-iBECs exposed to ultrasound (A, 0.3 MPa; B, 0.15 MPa) and stained immediately (Imm.) after treatment (UT, MB, US, US + MB, 20 $\times$  magnification, DAPI counterstain). Scale bar, 100  $\mu$ m,  
 (C) TEER ( $\Omega$ /cm<sup>2</sup>) in isogenic COR- and AD-iBECs in UT and US + MB conditions (0.3 MPa) immediately after treatment shown as fold change to UT (n = 6 from two independent experiments with two isogenic pairs).  
 (D) TEER ( $\Omega$ /cm<sup>2</sup>) in isogenic COR- and AD-iBECs in UT and US + MB conditions (0.15 MPa) immediately after treatment shown as fold change to UT (n = 6 from two independent experiments with two isogenic pairs).  
 (E) MTT cytotoxicity assay on UT- and US + MB-treated iBECs at 0.3 and 0.15 MPa rarefactional pressure (Imm.).  
 Data are presented as mean  $\pm$  SEM. Statistical analysis between two groups was performed using Student's t test and between multiple groups using one-way ANOVA, \*p < 0.05, \*\*p < 0.01, \*\*\*\*p < 0.0001. See also Figure S4.



(legend on next page)



COR-iBECs with an increased trend also observed in AD-iBEC US + MB condition (fold change 1.7) (Figure 7B). No significant difference in permeability was identified between the US + MB conditions in isogenic COR- and AD-iBECs (Figure 7B). We also found increased permeability of both isogenic COR-iBECs and AD-iBECs with the lower rarefactional pressure (0.15 MPa) US + MB treatment (Figure S5D).

Twenty-four hours after ultrasound treatment (0.3 MPa) the same iBEC cultures were exposed to dextran again, with no difference in dextran leakage observed between UT and US + MB conditions in isogenic COR-iBECs, supporting recovery of barrier integrity (Figure 7C). In contrast, 24 h after treatment, AD-iBECs demonstrated a persisting increased permeability to dextran in the US + MB condition compared with UT (Figure 7C). Dextran permeability in the AD-iBEC US + MB condition was also higher when compared with isogenic COR-iBEC UT and US + MB conditions (Figure 7C). As above, the same effect was observed at the lower pressure of 0.15 MPa (Figure S5E), indicating that increased permeability to dextran in AD-iBECs 24 h after treatment was not associated with the formation of cell-free spaces that were observed immediately after treatment at the higher pressure of 0.3 MPa.

Next, fluorescently conjugated A $\beta$ 1-42 (A $\beta$ ) was added to iBEC cultures immediately after 0.3 MPa ultrasound treatment and incubated for 24 h, after which the media in the top and bottom chamber of the Transwell were analyzed for fluorescence. In isogenic COR-iBECs, no difference in A $\beta$  leakage was identified after US + MB compared with the UT condition (Figure 7D). Intriguingly, AD-iBEC cultures demonstrated a strong increase in A $\beta$  permeability after US + MB compared with the UT condition (Figure 7D). Increased A $\beta$  leakage through the AD-iBEC monolayer after US + MB treatment was also identified when compared with isogenic COR-iBEC UT and US + MB conditions (Figure 7D). These results correlated with the permeability to dextran at 24 h and suggested impaired recovery of the AD-iBEC monolayer after US + MB treatment. US and MB alone conditions did not induce permeability to A $\beta$  (Figure S5).

## DISCUSSION

The BBB protects the brain from toxins and infectious agents, although even under physiological conditions there is an inherent “leakiness” allowing limited passage of some large molecules (Golde, 2014). Perturbations to the BBB have been reported in AD, but how this contributes to disease remains largely unknown (Sweeney et al., 2018). Advances in iPSC technology to generate human BECs provide new opportunities to explore BBB pathology in AD (Qian et al., 2017). Here, we established a model of the AD-BBB, by generating iBECs from FAD patient-derived hiPSCs harboring the *PSEN1*  $\Delta E9$  mutation, correcting the mutation to generate isogenic controls, and further, including cells from healthy individuals. We found that AD-iBECs exhibited differences both at the expression and functional level compared with ctrl-iBECs, reinforcing the notion of disease-specific impairments at the BBB. We also examined the cell response to therapeutic ultrasound with our results showing the ability of FUS together with MBs to open the iBEC tight junctions as a potential means for enhanced drug delivery across the BBB. Importantly, AD- and isogenic COR-iBECs responded differently to FUS, highlighting differences in the *PSEN1* mutant BBB and the importance of disease-specific models to develop drug delivery. Although iBECs can provide information on disease-specific differences at a cell-type-specific level, in the complete BBB, iBECs interact with astrocytes and pericytes, which may modulate how the disease mutation influences BBB function.

BBB breakdown in AD has been broadly reported (reviewed in Montagne et al., 2017) with our results supporting reduced BBB integrity in FAD for small molecules, with *PSEN1* mutant AD-iBECs exhibiting lower TEER compared with ctrl-iBECs. Interestingly, our analysis of TJP expression identified key differences between AD- and ctrl-iBECs, with both up- and downregulated genes, suggesting an altered brain endothelial phenotype in *PSEN1* mutation AD. It is possible that these changes are specific to *PSEN1* mutations and are not represented in other forms (i.e., late-onset sporadic) of AD. Our central findings are that in *PSEN1* mutant AD- compared with combined ctrl-iBECs,

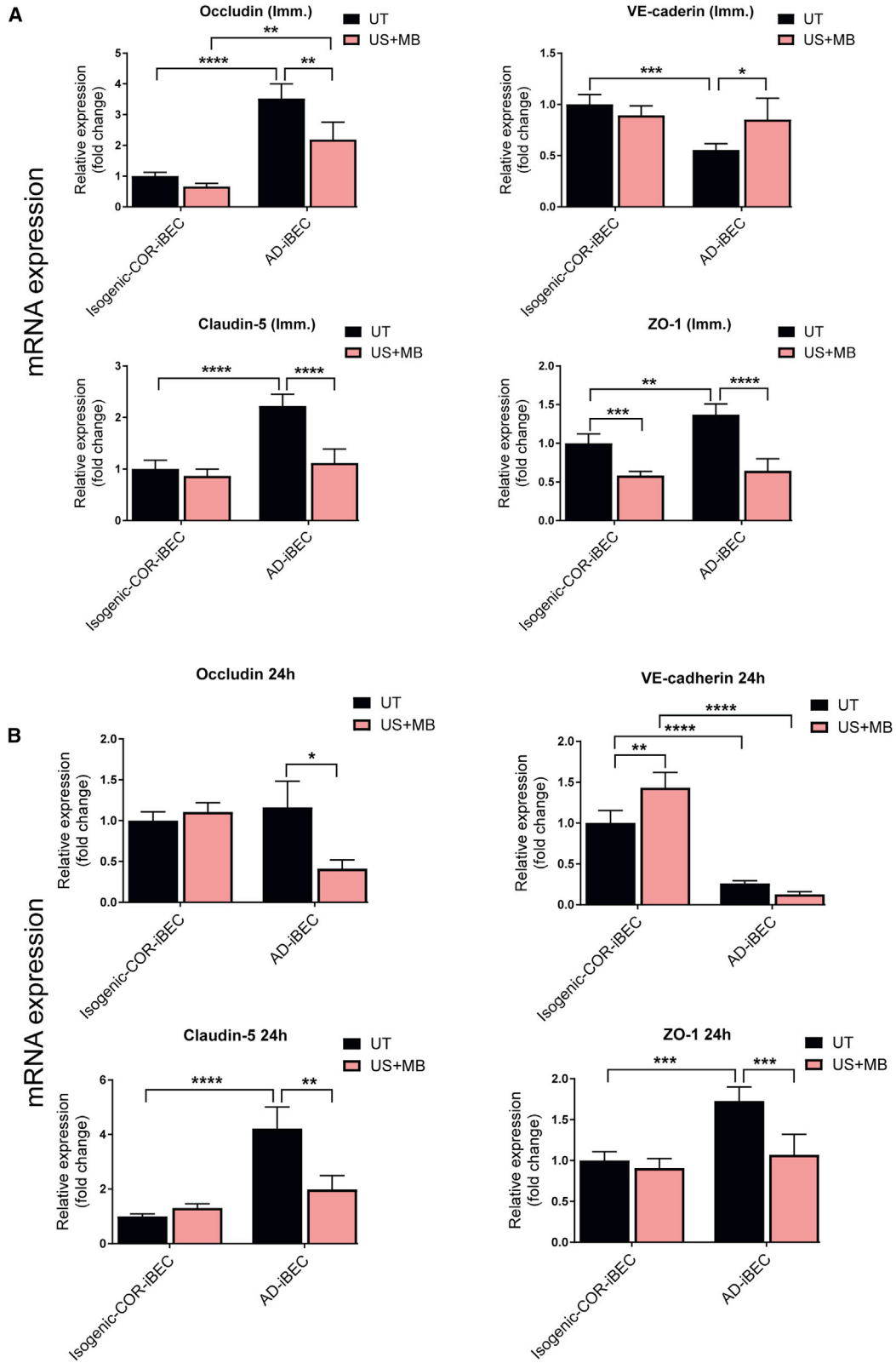
### Figure 5. iBEC Monolayer Recovers 24 h after Ultrasound Treatment

(A) Representative immunofluorescence images of claudin-5 (red) and occludin (green) along with co-stain in isogenic COR- and AD-iBECs exposed to US + MB and stained 24 h after treatment (20 $\times$  magnification, DAPI counterstain). Scale bar, 100  $\mu$ m.

(B) TEER ( $\Omega$ /cm<sup>2</sup>) in isogenic COR- and AD-iBECs in UT and US + MB conditions 24 h after treatment shown as fold change to UT condition (n = 6 from two independent experiments with two isogenic pairs). Data are presented as mean  $\pm$  SEM. Statistical analysis was performed using Student's t test, \*p < 0.05.

(C) Mean signal intensity of claudin-5 and occludin immediately and 24 h after US + MB treatment in isogenic COR- and AD-iBECs shown as fold change to isogenic corrected UT condition (n = 9 from three independent experiments with two isogenic pairs).

Data are presented as mean  $\pm$  SEM. Statistical analysis was performed using two-way ANOVA, \*p < 0.05, \*\*p < 0.01, \*\*\*p < 0.001, \*\*\*\*p < 0.0001. Only relevant differences are shown. See also Figure S4.



(legend on next page)

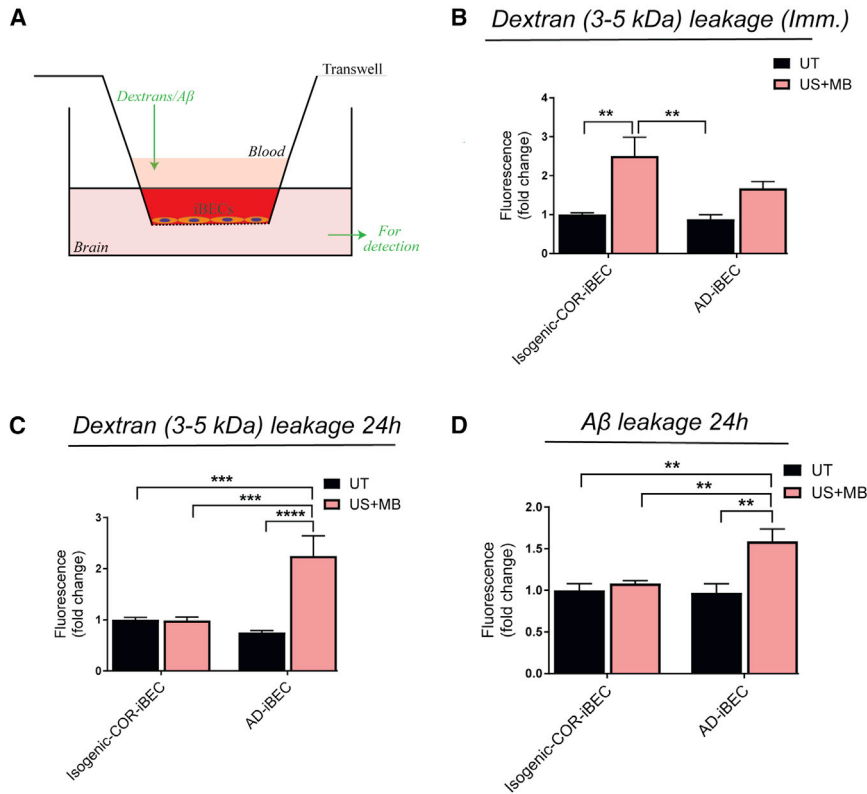


**Figure 7. FUS Increases the Permeability of the iBEC Monolayer to 3–5-kDa Dextran and Aβ with AD-iBECs Demonstrating Sustained Permeability 24 h after Treatment**

(A–C) (A) Assay of fluorescent dextran and Aβ leakage across iBECs in Transwells. Fluorescent dextran (3–5 kDa) leakage in isogenic COR- and AD-iBECs (B) immediately and (C) 24 h after US + MB treatment (0.3 MPa).

(D) Fluorescently conjugated Aβ leakage in isogenic COR- and AD-iBECs 24 h after US + MB treatment (0.3 MPa). Results shown as fold change to isogenic COR-iBEC UT condition (n = 3 independent replicates with two isogenic pairs).

Data are presented as mean ± SEM. Statistical analysis was performed using two-way ANOVA, \*\*p < 0.01, \*\*\*p < 0.001, \*\*\*\*p < 0.0001. Only relevant differences are shown. See also Figure S5.

mRNA levels for VE-cadherin were reduced, and claudin-3 and claudin-5 mRNA was increased, with increased claudin-5 expression also being confirmed by immunofluorescence. Reduced VE-cadherin expression in an AD mouse model and in postmortem tissue of AD patients has been reported (Lee et al., 2018). VE-cadherin is a key component of adherens junctions and its loss increases vascular permeability (Lee et al., 2018; Zenaro et al., 2017). In contrast, claudin-3 and claudin-5 are both key barrier-forming claudins (Gunzel and Yu, 2013); thus, their reduced expression in AD could cause observed reduction in BBB integrity. Interestingly, claudin-3 may not be expressed in BBB endothelial cells in mice (Castro Dias et al., 2019), although there are species differences between mice and human BBBs (O’Brown et al., 2018), and claudin-3 is expressed in human immortalized BECs (Schrade et al., 2012). Therefore, it is possible that claudin-3 may have other important functions in BECs.

Postmortem brain analysis has revealed decreased claudin-5 expression (Keaney et al., 2015; Yamazaki et al.,

2019); however, the opposite has also been reported (Romanitan et al., 2010). Changes to claudin-5 and other TJPs in AD may be driven by Aβ (Chao et al., 2016; Lee et al., 2018; Yamazaki et al., 2019). We observed that AD-iBECs with a *PSEN1* mutation expressed higher levels of some TJPs compared with healthy iBECs. It is unclear how these changes would affect the BBB. Higher expression could increase integrity but may have other outcomes, and this is supported by the lower TEER reading in AD-iBECs. Altered TJP expression can affect Aβ clearance from the brain. This was supported by downregulation of occludin and claudin-5 in the Tg2576 AD mouse model resulting in increased Aβ clearance (Keaney et al., 2015). Scanning ultrasound treatment of the APP23 AD mouse model led to transient opening of the BBB, but enhanced Aβ clearance was mediated via microglia rather than increased clearance to blood (Leinenga and Götz, 2015). In these mice, cognition was restored to wild-type levels. It remains to be determined how AD-iBECs would respond on Aβ after ultrasound treatment if microglia were added to the system.

**Figure 6. FUS Downregulates TJP mRNA with Reduced Recovery of AD-iBECs mRNA Levels**

Relative expression of mRNA for occludin, VE-cadherin, claudin-5, and ZO-1 in isogenic COR- and AD-iBECs (A) immediately and (B) 24 h after US + MB treatment (0.3 MPa) shown as fold change to isogenic COR-iBEC UT condition (n = 9 from three independent experiments with two isogenic pairs). Data are presented as mean ± SEM. Statistical analysis was performed using two-way ANOVA, \*p < 0.05, \*\*p < 0.01, \*\*\*p < 0.001, \*\*\*\*p < 0.0001. Only relevant differences are shown.



Our findings may also have implications for cerebral amyloid angiopathy (CAA), which is a common characteristic of AD (Andreas Charidimou et al., 2017). CAA can result from, as well as, exacerbate AD-related BBB dysfunction. Brain microvessels isolated from transgenic mouse models of AD and CAA reveal increased BBB leakage, and altered expression of TJPs (Magaki, et al., 2018). More recently it has been shown in aged APP23 mice that ultrasound treatment did not cause increased CAA or microbleeds, but cleared interstitial A $\beta$  effectively (Leinenga and Götz, 2018). Further studies are needed to determine if the PSEN1-mediated changes to iBEC integrity and TJP expression modulate or are affected by CAA.

In our study, A $\beta$  generation by iBECs was not measured. Although endothelial cells have the capacity to generate A $\beta$  (Placido et al., 2015), there is little understanding of how PSEN1 mutations affect A $\beta$  turnover in this cell type. It is not known whether increased A $\beta$ , or an alternative role for the PSEN1 mutation in the AD-iBECs, led to the observed changes in some TJP expression compared with healthy ctrl-iBECs. There are no reports of direct processing of TJPs by presenilin 1; however, presenilin 1 modulates Notch signaling via the  $\gamma$ -secretase complex (De Strooper et al., 1999). Notch signaling can alter BBB permeability through effects on TJPs (Ma et al., 2017). The specificity of these affects for AD-iBECs from patients with PSEN1 mutations should be further investigated by comparison with iBECs generated from patients with alternative PSEN and APP mutations, and ApoE isoforms.

We also identified differences in transporter expression in AD-iBECs, implying altered transport across the BBB in AD. Reduced GLUT-1 expression occurs in AD patients and animal models (Hooijmans et al., 2007; Vogelsang et al., 2018); however, we did not identify differences between AD- and combined ctrl-iBECs. We did find reduced expression and function of the efflux transporter P-gp in AD-iBECs, supporting previous findings in AD mouse models and human patients. Decreased P-gp expression correlates with increased A $\beta$  accumulation in mouse models of AD (Vogelgesang et al., 2002; Wang et al., 2016) and imaging of brains of patients with mild AD demonstrated reduced P-gp activity compared with controls (Deo et al., 2014). This evidence supports a role for P-gp in A $\beta$  clearance from the brain, and our identified reduced P-gp expression in AD-iBECs supports a likely contribution of the altered P-gp to AD pathogenesis. MRP1, MRP2, and BCRP efflux transporters were also increased in AD-iBECs compared with controls. The transporters belong to the family of ATP-cassette (ABC) transporters that play a major role in inhibiting the entry of drugs into the CNS (Qosa et al., 2015). Interestingly, Xiong et al. (2009) reported an upregulation of BCRP in the brains of AD patients, supporting our findings. Both P-gp and

BCRP are suggested to play a role in A $\beta$  transport across the BBB (Tai et al., 2009), suggesting the altered expression of these efflux transporters could contribute to abnormal A $\beta$  homeostasis in the brain. In addition, oxidative stress has been shown to increase ABC transporter expression at the BBB, hypothesized to be required to remove detoxification products (Wang et al., 2014). With oxidative stress associated with AD progression, it could explain increased efflux transporter expression in our model (Chen et al., 2012). More functional analyses of the role of transporter activity in BECs is important to understand the consequences on AD progression and drug delivery.

FUS has shown promising effects in tau-specific antibody delivery into the brain as well as in reducing A $\beta$  plaque and tau load in mouse models of AD (Leinenga and Götz, 2015; Nisbet et al., 2017; Pandit et al., 2019b). In addition, ultrasound treatment was safe in a number of animal models (Baseri et al., 2010; Blackmore et al., 2018; Leinenga et al., 2016). Therefore, FUS combined with MBs is a promising method for more efficient drug delivery across the BBB. As the effects of FUS in a human disease-specific BBB model remain sparsely investigated, we examined effects of FUS in our human model. We demonstrate for the first time the ability of FUS with MBs to disrupt an iBEC monolayer with recovery 24 h after treatment. The effects of FUS + MB treatment were clearly different on monolayer opening and permeability in AD- compared with isogenic COR-iBECs. Unexpectedly, our data suggest that the AD-iBEC monolayer is more resilient to immediate effects of FUS, but recovers more slowly from treatment compared with isogenic COR-iBECs. The resistance demonstrated by AD-iBECs to FUS treatment could be due to increased claudin expression as discussed above.

We also show that US + MB increased permeability of iBEC monolayers to 3–5-kDa sized dextrans and A $\beta$ . Although the compounds were added to the apical side, corresponding to the blood side in the body, A $\beta$  flux across the BBB is reported to be bidirectional (Wang et al., 2016), suggesting that FUS has a potential to clear A $\beta$  also from the basolateral side. Importantly, 24 h after FUS treatment permeability to dextrans and A $\beta$  remained high in AD-iBECs while it recovered in isogenic COR-iBECs. The transport of larger molecules has not been explored by us. Within the limitation of our study that assessed a particular familial mutation of AD, in a clinical setting, an advantage could be a more efficient clearance of A $\beta$  from AD brains or the more efficient delivery of therapeutic drugs. This highlights the importance of investigating disease-specific effects of FUS on the BBB, but also asks for validation in an *in vivo* model to integrate findings made in *in vitro* and *in vivo* systems. A recent trial proved safety of FUS-mediated BBB opening in five patients with early to moderate AD (Lipsman et al., 2018), and a second trial showed that



even implanted transducers were tolerated in patients with glioblastomas, without inducing neurotoxicity (Idbaih et al., 2019). With FUS shown to induce A $\beta$  internalization by microglia (Leinenga and Götz, 2015), in future studies a human *in vitro* model that comprises key BBB and brain cells, including BECs, pericytes, astrocytes and microglia, would be useful.

In conclusion, our results demonstrate that *PSEN1* mutant AD-iBECs harbor phenotypical differences elucidating disease-specific effects on the BBB in AD. In addition, we show that these cells provide an excellent complementary model to investigate new means of drug delivery and to understand how the BBB can be exploited for the treatment of AD.

## EXPERIMENTAL PROCEDURES

### hiPSC Expansion and iBEC Differentiation

Six hiPSC lines were used, including three FAD lines harboring the *PSEN1* exon 9 deletion (Oksanen et al., 2017), two corresponding isogenic gene-corrected control lines (Oksanen et al., 2017), and one unrelated healthy control line HDFa reprogrammed from adult dermal fibroblasts (HDFa, Gibco, C0135C) using the CytoTune-iPS 2.0 Sendai Reprogramming Kit (Invitrogen, A16518). Details of the HDFa line generation are provided in Supplemental Experimental Procedures. All hiPSC lines were maintained on human recombinant vitronectin in StemFlex medium (Life Technologies). Differentiation was performed as described previously (Qian et al., 2017; Stebbins et al., 2016) with some modification, and is described in detail in Supplemental Experimental Procedures. The work was approved by the QIMR Berghofer Human Ethics Committee.

### FUS

FUS experiments were performed on two AD and two respective isogenic (corrected) control lines. The effect of ultrasound was tested on iBECs 48–72 h after subculture. For immunofluorescent detection, cells were grown on 24-well plates, and for TEER and permeability assays cells were grown on Transwell inserts. Two time points were used (immediately and 24 h after ultrasound) and cells were tested under four conditions: (1) UT, (2) MB control, (3) US control, and (4) test condition (US + MB), which received both ultrasound and MBs. MBs were prepared as described previously (Leinenga and Götz, 2015) and added to the wells aseptically (10  $\mu$ L per well). Cells were then exposed to the ultrasound transducer (Sonic Concepts H117) using the following parameters: 0.3 or 0.15 MPa peak rarefactional pressure, 50 cycles/burst, burst period 20 ms, 286 Hz center frequency, and a 120-s sonication time. For the US condition, cells were sonicated at the same parameters without MBs. For the MB condition, MBs were added to the individual wells for 120 s and no ultrasound was performed.

### Dextran and A $\beta$ Leakage Analysis

To examine the barrier integrity of the iBEC monolayer after ultrasound treatment, the permeability to fluorescein isothiocyanate

(FITC)-conjugated dextran molecules of 3–5 kDa (Sigma) and FITC-conjugated A $\beta$ <sub>42</sub> (Bachem) in Transwell inserts was analyzed. For dextran leakage, after ultrasound exposure, the top chamber medium was removed and replaced with medium containing 0.5 mg/mL of dextrans. For the 0-h time point, dextrans were added on inserts immediately after ultrasound and bottom chamber medium collected for analysis after 30 min. Culture medium in both top and bottom chambers was then replaced with fresh medium and after 24 h recovery dextrans were added again to the top chamber and incubated for 30 min as in the immediate time point. To examine leakage of A $\beta$  through the iBEC monolayer after ultrasound treatment, top chamber medium was removed and replaced with culture medium containing 5  $\mu$ M of FITC-A $\beta$ . Cells were incubated with FITC-A $\beta$  for 24 h, after which the top and bottom chamber media were collected for analysis. Fluorescence of both dextrans and A $\beta$  was measured using a fluorescent plate reader (Biotek Synergy H4) at 490 nm excitation/520 nm emission wavelengths. For analysis of A $\beta$  leakage, the ratio of bottom/top chamber fluorescence was calculated.

### Statistical Analysis

Statistical analysis was performed with GraphPad Prism 7.02 using Student's t test, one-way ANOVA with Tukey's multiple comparison test, or two-way ANOVA with Sidak's multiple comparison test. Statistical significance was determined as \* $p < 0.05$ , \*\* $p < 0.01$ , \*\*\* $p < 0.001$ , \*\*\*\* $p < 0.0001$ . All data are presented as mean  $\pm$  SEM.

## SUPPLEMENTAL INFORMATION

Supplemental Information can be found online at <https://doi.org/10.1016/j.stemcr.2020.03.011>.

## AUTHOR CONTRIBUTIONS

L.E.O. designed and performed most experiments, analyzed the data, and wrote the manuscript. R.P. and J.G. designed ultrasound experiments and edited the manuscript. R.P. performed ultrasound experiments and analyzed the data. R.Stewart generated iBEC cultures and helped with experimental design. R.Sutharsan helped with ultrasound experiments. C.C.-L. and L.M.R. extracted RNA and performed qPCR. H.Q. provided technical assistance across multiple experiments. C.M.d.B. and J.M.P. generated and provided the HDFa iPSC line. M.O., S.L., and J.K. generated, characterized, and provided the AD and isogenic iPSC lines, and contributed to endothelial differentiation. A.R.W. designed the experiments, interpreted the data, and edited the manuscript.

## ACKNOWLEDGMENTS

We thank the Genomics Research Center (IHBI, QUT) for technical assistance. We also thank Dr Liyu Chen (Queensland Brain Institute) for additional technical assistance. This research was supported by QIMR Berghofer SEED grant (to L.E.O.), NHMRC Project grants APP1125796 (to A.R.W.), and GNT1145580 (to J.G.). A.R.W. is a recipient of an NHMRC Senior Research Fellowship (APP1118452). The project is supported through the Academy of Finland under the aegis of JPND—[www.jpnd.eu](http://www.jpnd.eu)—and European



Union's Horizon 2020 research and innovation program under grant agreement no. 643417 (to J.K.).

Received: June 18, 2019

Revised: March 11, 2020

Accepted: March 12, 2020

Published: April 9, 2020

## REFERENCES

- Andreas Charidimou, A., Boulouis, G., Gurol, M.E., Ayata, C., Bacsakai, B.J., Frosch, M.P., Viswanathan, A., and Greenberg, S.M. (2017). Emerging concepts in sporadic cerebral amyloid angiopathy. *Brain* 140, 1829–1850.
- Baseri, B., Choi, J.J., Tung, Y.S., and Konofagou, E.E. (2010). Multimodality safety assessment of blood-brain barrier opening using focused ultrasound and definity microbubbles: a short-term study. *Ultrasound Med. Biol.* 36, 1445–1459.
- Bien-Ly, N., Boswell, C.A., Jeet, S., Beach, T.G., Hoyte, K., Luk, W., Shihadeh, V., Ulufatu, S., Foreman, O., Lu, Y., et al. (2015). Lack of widespread BBB disruption in Alzheimer's disease models: focus on therapeutic antibodies. *Neuron* 88, 289–297.
- Blackmore, D.G., Turpin, F., Mohamed, A.Z., Zong, F., Pandit, R., Pelekanos, M., Nasrallah, F., Sah, P., Bartlett, P.F., and Götz, J. (2018). Multimodal analysis of aged wild-type mice exposed to repeated scanning ultrasound treatments demonstrates long-term safety. *Theranostics* 8, 6233–6247.
- Castro Dias, M., Coisne, C., Baden, B., Enzmann, G., Garrett, L., Becker, L., Hölter, S.M., German Mouse Clinic Consortium, Hrabě de Angelis, M., Deutsch, U., and Engelhardt, E. (2019). Claudin-12 is not required for blood–brain barrier tight junction function. *Fluids Barriers CNS* 16, 30.
- Chao, A.C., Lee, T.C., Juo, S.H., and Yang, D.I. (2016). Hyperglycemia increases the production of amyloid beta-peptide leading to decreased endothelial tight junction. *CNS Neurosci. Ther.* 22, 291–297.
- Chen, X., Guo, C., and Kong, J. (2012). Oxidative stress in neurodegenerative diseases. *Neural Regen. Res.* 7, 376–385.
- Deo, A.K., Borson, S., Link, J.M., Domino, K., Eary, J.F., Ke, B., Richards, T.L., Mankoff, D.A., Minoshima, S., O'Sullivan, F., et al. (2014). Activity of P-glycoprotein, a beta-amyloid transporter at the blood-brain barrier, is compromised in patients with mild Alzheimer disease. *J. Nucl. Med.* 55, 1106–1111.
- Devraj, K., Klinger, M.E., Myers, R.L., Mokashi, A., Hawkins, R.A., and Simpson, I.A. (2011). GLUT-1 glucose transporters in the blood-brain barrier: differential phosphorylation. *J. Neurosci. Res.* 89, 1913–1925.
- Frezza, R.L., Lourenco, M.V., and De Felice, F.G. (2018). Challenges for Alzheimer's disease therapy: insights from novel mechanisms beyond memory defects. *Front. Neurosci.* 12, 37.
- Gama Sosa, M.A., Gasperi, R.D., Rocher, A.B., Wang, A.C., Janssen, W.G., Flores, T., Perez, G.M., Schmeidler, J., Dickstein, D.L., Hof, P.R., et al. (2010). Age-related vascular pathology in transgenic mice expressing presenilin 1-associated familial Alzheimer's disease mutations. *Am. J. Pathol.* 176, 353–368.
- Golde, T.E. (2014). Open questions for Alzheimer's disease immunotherapy. *Alzheimers Res. Ther.* 6, 3.
- Gunzel, D., and Yu, A.S. (2013). Claudins and the modulation of tight junction permeability. *Physiol. Rev.* 93, 525–569.
- Hooijmans, C.R., Graven, C., Dederen, P.J., Tanila, H., van Groen, T., and Kiliaan, A.J. (2007). Amyloid beta deposition is related to decreased glucose transporter-1 levels and hippocampal atrophy in brains of aged APP/PS1 mice. *Brain Res.* 1181, 93–103.
- Hultman, K., Strickland, S., and Norris, E.H. (2013). The APOE varepsilon4/varepsilon4 genotype potentiates vascular fibrin(ogen) deposition in amyloid-laden vessels in the brains of Alzheimer's disease patients. *J. Cereb. Blood Flow Metab.* 33, 1251–1258.
- Idbaih, A., Canney, M., Belin, L., Desseaux, C., Vignot, A., Bouchoux, G., Asquier, N., Law-Ye, B., Leclercq, D., Bissery, A., et al. (2019). Safety and feasibility of repeated and transient blood-brain barrier disruption by pulsed ultrasound in patients with recurrent glioblastoma. *Clin. Cancer Res.* 25, 3793–3801.
- Jordao, J.F., Ayala-Grosso, C.A., Markham, K., Huang, Y., Chopra, R., McLaurin, J., Hynynen, K., and Aubert, I. (2010). Antibodies targeted to the brain with image-guided focused ultrasound reduces amyloid-beta plaque load in the TgCRND8 mouse model of Alzheimer's disease. *PLoS One* 5, e10549.
- Keaney, J., Walsh, D.M., O'Malley, T., Hudson, N., Crosbie, D.E., Loftus, T., Sheehan, F., McDaid, J., Humphries, M.M., Callanan, J.J., et al. (2015). Autoregulated paracellular clearance of amyloid- $\beta$  across the blood-brain barrier. *Sci. Adv.* 1, e1500472.
- Lee, D., Cho, S.-J., Lim, H.J., Seok, J., Jo, C., Jo, S.A., Park, M.H., Han, C., Kowall, N., Ryu, H., et al. (2018). Alteration of vascular endothelial cadherin in Alzheimer's disease patient and mouse model. *bioRxiv* <https://doi.org/10.1101/430140>.
- Leinenga, G., and Götz, J. (2015). Scanning ultrasound removes amyloid-beta and restores memory in an Alzheimer's disease mouse model. *Sci. Transl. Med.* 7, 278ra233.
- Leinenga, G., and Götz, J. (2018). Safety and efficacy of scanning ultrasound treatment of aged APP23 mice. *Front. Neurosci.* 12, 55.
- Leinenga, G., Langton, C., Nisbet, R., and Götz, J. (2016). Ultrasound treatment of neurological diseases—current and emerging applications. *Nat. Rev. Neurol.* 12, 161–174.
- Li, W., Chen, Z., Chin, I., Chen, Z., and Dai, H. (2018). The role of VE-cadherin in blood-brain barrier integrity under central nervous system pathological conditions. *Curr. Neuropharmacol.* 16, 1375–1384.
- Lippmann, E.S., Al-Ahmad, A., Azarin, S.M., Palecek, S.P., and Shusta, E.V. (2014). A retinoic acid-enhanced, multicellular human blood-brain barrier model derived from stem cell sources. *Sci. Rep.* 4, 4160.
- Lipsman, N., Meng, Y., Bethune, A.J., Huang, Y., Lam, B., Masellis, M., Herrmann, N., Heyn, C., Aubert, I., Boutet, A., et al. (2018). Blood-brain barrier opening in Alzheimer's disease using MR-guided focused ultrasound. *Nat. Commun.* 9, 2336.
- Ma, S.C., Li, Q., Peng, J.Y., Zhouwen, J.L., Diao, J.F., Niu, J.X., Wang, X., Guan, X.D., Jia, W., and Jiang, W.G. (2017). Claudin-5 regulates blood-brain barrier permeability by modifying brain microvascular endothelial cell proliferation, migration, and adhesion to prevent lung cancer metastasis. *CNS Neurosci. Ther.* 23, 947–960.
- Magaki, S., Tang, Z., Tung, S., Williams, C.K., Lo, D., Yong, W.H., Khanlou, N., and Vinters, H.V. (2018). The effects of cerebral



amyloid angiopathy on integrity of the blood-brain barrier. *Neurobiol. Aging* 70, 70–77.

Montagne, A., Zhao, Z., and Zlokovic, B.V. (2017). Alzheimer's disease: a matter of blood-brain barrier dysfunction? *J. Exp. Med.* 214, 3151–3169.

Nelson, A.R., Sweeney, M.D., Sagare, A.P., and Zlokovic, B.V. (2016). Neurovascular dysfunction and neurodegeneration in dementia and Alzheimer's disease. *Biochim. Biophys. Acta* 1862, 887–900.

Nisbet, R.M., Van der Jeugd, A., Leinenga, G., Evans, H.T., Janowicz, P.W., and Götz, J. (2017). Combined effects of scanning ultrasound and a tau-specific single chain antibody in a tau transgenic mouse model. *Brain* 140, 1220–1230.

O'Brown, N.M., Pfau, S.J., and Gu, C. (2018). Bridging barriers: a comparative look at the blood-brain barrier across organisms. *Genes Dev.* 32, 466–478.

Oksanen, M., Petersen, A.J., Naumenko, N., Puttonen, K., Lehtonen, S., Gubert Olive, M., Shakirzyanova, A., Leskela, S., Sarajarvi, T., Viitanen, M., et al. (2017). PSEN1 mutant iPSC-derived model reveals severe astrocyte pathology in Alzheimer's disease. *Stem Cell Reports* 9, 1885–1897.

Pandit, R., Chen, L., and Götz, J. (2019a). The blood-brain barrier: physiology and strategies for drug delivery. *Adv. Drug Deliv. Rev.* <https://doi.org/10.1016/j.addr.2019.11.009>.

Pandit, R., Leinenga, G., and Götz, J. (2019b). Repeated ultrasound treatment of tau transgenic mice clears neuronal tau by autophagy and improves behavioral functions. *Theranostics* 9, 3754–3767.

Placido, A.I., Oliveira, C.R., Moreira, P.I., and Pereira, C.M. (2015). Enhanced amyloidogenic processing of amyloid precursor protein and cell death under prolonged endoplasmic reticulum stress in brain endothelial cells. *Mol. Neurobiol.* 51, 571–590.

Polanco, J.C., Li, C., Bodea, L.G., Martinez-Marmol, R., Meunier, F.A., and Götz, J. (2018). Amyloid-beta and tau complexity—towards improved biomarkers and targeted therapies. *Nat. Rev. Neurol.* 14, 22–39.

Qian, T., Maguire, S.E., Canfield, S.G., Bao, X., Olson, W.R., Shusta, E.V., and Palecek, S.P. (2017). Directed differentiation of human pluripotent stem cells to blood-brain barrier endothelial cells. *Sci. Adv.* 3, e1701679.

Qosa, H., Miller, D.S., Pasinelli, P., and Trotti, D. (2015). Regulation of ABC efflux transporters at blood-brain barrier in health and neurological disorders. *Brain Res.* 1628, 298–316.

Romanitan, M.O., Popescu, B.O., Spulber, S., Bajenaru, O., Popescu, L.M., Winblad, B., and Bogdanovic, N. (2010). Altered expression of claudin family proteins in Alzheimer's disease and vascular dementia brains. *J. Cell Mol. Med.* 14, 1088–1100.

Ryan, N.S., Nicholas, J.M., Weston, P.S.J., Liang, Y., Lashley, T., Guerreiro, R., Adamson, G., Kenny, J., Beck, J., Chavez-Gutierrez, L., et al. (2016). Clinical phenotype and genetic associations in autosomal dominant familial Alzheimer's disease: a case series. *Lancet Neurol.* 15, 1326–1335.

Schrade, A., Sade, H., Couraud, P., Romero, I.A., Weksler, B.B., and Niewoehner, J. (2012). Expression and localization of claudins-3

and -12 in transformed human brain endothelium. *Fluids Barriers CNS* 9, 6.

Sheikov, N., McDannold, N., Vykhodtseva, N., Jolesz, F., and Hynynen, K. (2004). Cellular mechanisms of the blood-brain barrier opening induced by ultrasound in presence of microbubbles. *Ultrasound Med. Biol.* 30, 979–989.

Stebbins, M.J., Wilson, H.K., Canfield, S.G., Qian, T., Palecek, S.P., and Shusta, E.V. (2016). Differentiation and characterization of human pluripotent stem cell-derived brain microvascular endothelial cells. *Methods* 101, 93–102.

De Strooper, B., Annaert, W., Cupers, P., Saftig, P., Craessaerts, K., Mumm, J.S., Schroeter, E.H., Schrijvers, V., Wolfe, M.S., Ray, W.J., et al. (1999). A presenilin-1-dependent gamma-secretase-like protease mediates release of Notch intracellular domain. *Nature* 398, 518–522.

Sweeney, M.D., Sagare, A.P., and Zlokovic, B.V. (2018). Blood-brain barrier breakdown in Alzheimer disease and other neurodegenerative disorders. *Nat. Rev. Neurol.* 14, 133–150.

Tai, L.M., Loughlin, A.J., Male, D.K., and Romero, I.A. (2009). P-glycoprotein and breast cancer resistance protein restrict apical-to-basolateral permeability of human brain endothelium to amyloid-beta. *J. Cereb. Blood Flow Metab.* 29, 1079–1083.

Vogelgesang, S., Cascorbi, I., Schroeder, E., Pahnke, J., Kroemer, H.K., Siegmund, W., Kunert-Keil, C., Walker, L.C., and Warzok, R.W. (2002). Deposition of Alzheimer's beta-amyloid is inversely correlated with P-glycoprotein expression in the brains of elderly non-demented humans. *Pharmacogenetics* 12, 535–541.

Vogelsang, P., Giil, L.M., Lund, A., Vedeler, C.A., Parkar, A.P., Nordrehaug, J.E., and Kristoffersen, E.K. (2018). Reduced glucose transporter-1 in brain derived circulating endothelial cells in mild Alzheimer's disease patients. *Brain Res.* 1678, 304–309.

Wang, X., Campos, C.R., Peart, J.C., Smith, L.K., Boni, J.L., Cannon, R.E., and Miller, D.S. (2014). Nrf2 upregulates ATP binding cassette transporter expression and activity at the blood-brain and blood-spinal cord barriers. *J. Neurosci.* 34, 8585–8593.

Wang, W., Bodles-Brakhop, A.M., and Barger, S.W. (2016). A role for P-glycoprotein in clearance of Alzheimer amyloid beta -peptide from the brain. *Curr. Alzheimer Res.* 13, 615–620.

Xiong, H., Callaghan, D., Jones, A., Bai, J., Rasquinha, I., Smith, C., Pei, K., Walker, D., Lue, L.F., Stanimirovic, D., et al. (2009). ABCG2 is upregulated in Alzheimer's brain with cerebral amyloid angiopathy and may act as a gatekeeper at the blood-brain barrier for Abeta(1-40) peptides. *J. Neurosci.* 29, 5463–5475.

Yamazaki, A., Liesinger, A.M., Dickson, D.W., Murray, M.E., Shinohara, M., Shinohara, M., Kanekiyo, T., Yamazaki, Y., Bu, G., Lesser, E.R., et al. (2019). Selective loss of cortical endothelial tight junction proteins during Alzheimer's disease progression. *Brain* 142, 1077–1092.

Zenaro, E., Pietronigro, E., Della Bianca, V., Piacentino, G., Marongiu, L., Budui, S., Turano, E., Rossi, B., Angiari, S., Dusi, S., et al. (2015). Neutrophils promote Alzheimer's disease-like pathology and cognitive decline via LFA-1 integrin. *Nat. Med.* 21, 880–886.

Zenaro, E., Piacentino, G., and Constantin, G. (2017). The blood-brain barrier in Alzheimer's disease. *Neurobiol. Dis.* 107, 41–56.